

MODEL OF ASH SIZE DISTRIBUTIONS FROM COAL CHAR OXIDATION

Boyd F. Edwards and Anjan K. Ghosal

Department of Physics, West Virginia University
Morgantown, WV 26506

1. Abstract

A flexible model of final ash size distributions resulting from coal char oxidation under varying conditions is presented. To include the important effects of fragmentation during char oxidation, we have modeled three-dimensional char particles as porous spatially random "percolation" clusters on a cubic bond lattice. Random walkers represent oxygen diffusion to the surface of the char particles. A reaction probability r governs whether a random walker reaching the surface will react with a unit mass of char. Thus, values of r from near zero to unity take the model from a chemical-reaction-limited to a diffusion-limited regime. Fragmentation events occur when reactions break the connectivity of the clusters, leading to a distribution of ash particle sizes after burnout. In the chemistry-limited regime, penetration of the random walkers into the pores of the cluster results in major fragmentation events and a correspondingly large number of ash particles. In the diffusion-limited regime, the lack of such penetration results in fewer ash particles with a larger maximum size. Model parameters are related to experimental conditions such as temperature, particle diameter, char porosity, and ash content. Results are compared with experiments.

2. Introduction

Coals typically contain about 10% incombustible mineral matter mainly in small separate inclusions in the coal. During combustion these particles can be released into the furnace gases as fly ash and may range from a hundredth of a micron to up to a 100 microns in diameter. These ash particles clog heat transfer equipment, corrode boiler tubes and create environmental hazards. To fully address these problems, it is important to understand the mechanism of ash formation. In this paper, we present a model of coal char oxidation designed to supply this understanding. Our objective is to numerically simulate the effect of coal morphology, burning rate, and initial ash content on the final ash size distribution.

Recent measurements of burning-rate time histories for single char particles in a fluidized bed (1) offer new insights into the dynamics of the combustion process. Of particular interest are successive sharp increases in the burning rate interrupting the overall downward trend. These sharp increases were interpreted as the fragmentation of char particles or subparticles into two or more pieces, and were not observable in previous time-averaged or ensemble-averaged measurements.

Though useful in characterizing various oxidation regimes, standard models of char oxidation deemphasize fragmentation by treating char particles as uniform spheres (2,3), thereby simplifying the problem of oxygen diffusion to the surface. Subsequent models allow for fragmentation effects by treating char particles as random porous shapes. Reyes and Jensen (4,5) modeled char oxidation on a Bethe (tree-like) lattice by randomly removing bonds (unit line segments) from anywhere on the lattice. More realistically, Kerstein and Bug (6) randomly removed an initial fraction of bonds from the Bethe lattice to represent the porosity of the unburned char particle, and randomly removed only surface bonds to simulate oxidation. To account for loop effects (which are absent on the Bethe lattice), Sahimi and Tsotsis (7) studied surface bond removal on a porous three-dimensional site lattice in the chemistry limited regime (Zone I). A Zone III (diffusion-limited) model (8) accounted for the sharp increases in the burning-rate measurements, ascribing them to a higher burning rate per unit surface area of char fragments than their parent char particles. These models demonstrated the utility of modeling char particles as random "percolation" clusters on a three-dimensional cubic lattice.

Models of char oxidation and fragmentation to date neglect ash formation and force all particles into a particular regime (Zone I or Zone III) regardless of size. In contrast, the smallest particles in real combustion systems might be in Zone I (because of their higher surface oxygen concentration) while the larger particles are simultaneously in Zone III (2). The present model incorporates both regimes

along with the intermediate regime (Zone II), as well as incorporating ash formation.

Further measurements on a finely graded Montana lignite (9,10) with mass averaged mineral inclusion size of 2 microns indicate strong dependencies of the final ash size distribution on temperature, initial particle size, and oxygen concentration. In this paper, we directly compare the predictions of the model with these experiments.

3. Model

The distribution of ash particle sizes after complete burnout depends on the competition between several mechanisms. Mineral inclusions melt and can coalesce as the surface of the char particle recedes, leading to large ash particles. Small protrusions in the irregular char surface can be liberated as the surface recedes, producing small ash particles. In the chemistry-limited regime, oxygen diffusion and oxidation in the pores can lead to separation of char particles into particles of comparable size, leading to ash particles more evenly distributed in size. Finally, mineral vaporization at the surface and subsequent condensation can lead to very small ash particles (11). Since they solidify from liquid mineral droplets, ash particles are typically spherical or near spherical.

To incorporate the most important mechanisms of ash production into our model in a straightforward way, we employ a representation of char particles on a cubic lattice similar to one used in a previous model (8), except that here we include mineral matter in the representation. The lattice representation employs the site percolation concept; each site on a cubic lattice has probability $p = 0.3117$ of being "occupied". Groups of adjacent occupied sites are termed site clusters. This value of p is the "percolation threshold" value above which a cluster spanning the cubic site lattice is guaranteed to exist. All unit line segments, or "bonds", within a radius R of occupied sites are designated as solid. The resulting bond cluster represents a porous char particle whose compactness is governed by R . A fraction of the bonds in the cluster are assigned masses of mineral material to simulate mineral inclusions. Note that a bond is a line segment between nearest neighbor sites on a lattice, representing a mass of combustible and mineral material, and does not represent a chemical bond.

Char oxidation is modeled by introducing random walkers representing oxygen. Each time a random walker encounters a solid bond, that is, each time it crosses a solid bond, it has a probability r of reacting with the bond. A reaction is defined as the annihilation of both the walker and the combustible content of the bond. If an encounter does not lead to reaction, the walk continues from the point where it entered the solid. In this way, small values of r lead to many encounters before reaction occurs, allowing walkers to deeply penetrate the pores before reacting. A reaction that breaks the connectedness of a cluster is deemed a fragmentation event. After such an event, the random walkers ignore all solid bonds except those pertaining to a single fragment to simulate physically separated particles produced by fragmentation events, each with a separate supply of oxygen. The fragments are oxidized one at a time in this manner until all have been oxidized. The site lattice oxidation model by Sahimi and Tsois (7,12) apparently ignores this physical separation. Extension of the model to give the time-dependent char fragment size distribution during oxidation is in progress.

Two limiting behaviors for reallocating the mineral mass of a reacted bond are simulated as follows. Limit I: For strong cohesion between adjacent melted mineral inclusions, the mineral mass of a reacted bond is given to the adjacent solid bond with the largest mineral mass, giving strong coalescence of mineral matter. Limit II: In the opposite case of weak mineral cohesion and relatively strong adhesion between melted mineral inclusions and char material, the mineral mass of a reacted bond is equally divided among its adjacent solid bonds, giving weak coalescence. When the last solid bond of a cluster reacts, its mineral mass is deemed the mass of an ash particle. When all solid bonds have reacted, the ash mass distribution is complete. The corresponding ash size distribution follows from the sphericity of the ash particles. In this way, the model captures the effects on the ash distribution of surface coalescence, liberation of surface protrusions, and pore diffusion during oxidation. Although the model does not account for mineral vaporization (11), the very small submicron ash particles created by this mechanism are negligible in the final mass-weighted size distribution. We assume that the adhesion between melted mineral inclusions of different chemical compositions, if such differences occur in the coal being considered, can be treated as identical to the cohesion of inclusions of the same composition.

The advantage of using a bond lattice rather than a site lattice is the absence of unphysical spurious

multiple fragmentation events. Removing a single site from a cubic site lattice can result in up to 6 fragments, whereas removing a single bond from a cubic bond lattice results in no more than two fragments.

The reaction probability r depends on the particle diameter d through the oxygen diffusion rate K_d (see Section 4 below). Thus, it is necessary to define the diameter of a cluster on the cubic bond lattice which can be related to the actual particle diameter d . This "lattice diameter" d_l is defined as the average of the cluster dimensions in the three cartesian directions; $d_l = (x_{\max} - x_{\min} + y_{\max} - y_{\min} + z_{\max} - z_{\min}) / 3$, measured in units of the lattice spacing. The lattice spacing in microns, which remains fixed during the simulation, is determined initially by equating the initial particle diameter d (in microns) to the diameter d_l of the cluster used to simulate it (in lattice spacings). The diameter and the corresponding reaction probability r of a particular particle decrease monotonically from an initial value during oxidation, taking it into the chemistry-limited regime as it decreases in size. Cluster diameters and corresponding reaction probabilities are accordingly updated after each bond reacts.

Random walkers are introduced at random locations on a box with linear dimensions a factor of 1.4 larger than the dimensions of the box of dimensions $x_{\max} - x_{\min}$, $y_{\max} - y_{\min}$, and $z_{\max} - z_{\min}$. Tests to be described elsewhere indicate that this method of introducing random walkers yields probabilities of contacting particular solid bonds that are within 4% of the probabilities obtained by introducing the walkers an infinite distance from the cluster.

4. Relation of the reaction probability r to physical quantities

For a first-order reaction, the rate of consumption Q of carbon at the surface of a char particle of diameter d is proportional to the partial pressure C_s of oxygen at the surface through the relation $Q = K_c C_s$, where $K_c = A \exp(-E/RT_s)$ is the chemical reaction rate characterizing the chemisorption process. This oxygen at the surface arrives by diffusion across the relatively stagnant gas film between the bulk gas stream and the solid surface. The corresponding alternative relation $Q = K_d (C_b - C_s)$ involves the oxygen diffusion rate $K_d = B T_s^{0.75} / d$ (Refs. 13, 14). Since the bulk oxygen partial pressure C_b is the measurable quantity, a third relation $Q = K C_b$ defines the overall reaction rate K , which is simply related to its constituent rates as $K^{-1} = K_d^{-1} + K_c^{-1}$ by combining the three forms for Q . For very small surface temperatures T_s , $K = K_c$ and a small oxygen flux to the surface is sufficient to sustain the slow chemical reactions both at the external surface of the solid and deep within its pores (Zone I). At higher temperatures, oxygen is unable to diffuse into the pores fast enough to completely support the faster chemical reactions, but is plentiful at the external surface (Zone II). At yet higher temperatures, $K = K_d$ and oxygen diffusion is unable to completely support the chemical reactions even at the external surface (Zone III).

The foregoing assumes an order of reaction equal to unity. CO is typically the primary oxidation product in char combustion (2), but converts to CO₂ a distance from the particle. Experimental evidence that CO₂ is the combustion product most relevant to diffusion to and from char particles, and that the order of reaction is consequently close to unity, is given by Field (15) for pulverized chars with $0.05 \text{ atm} < C_b < 0.20 \text{ atm}$, and by Smith (13). Accordingly, we take $A = 8710 \text{ g cm}^{-2}\text{s}^{-1}\text{atm}^{-1}$, $E = 35700 \text{ cal/mole}$, and $R = 1.986 \text{ cal mole}^{-1} \text{ K}^{-1}$ (3), which apparently apply generally, to within the accuracy of our simulations, to coals excluding pyrolytic graphites and anthracites. The value $B = 5.62 \times 10^{-6} \text{ g cm}^{-2}\text{s}^{-1}\text{atm}^{-1}$ based on the external surface area (mass removed per unit external surface area per atmosphere of O₂ per unit time) follows from the corresponding mass-based coefficient given by Smith (13), which depends on the diffusivity of O₂ in air. More specific values of E , R , and A for various coal types are given by Wall and Gururajan (16).

The reaction probability r of the simulations follows simply from the overall reaction rate K . For r near zero, random walkers encounter the solid many times before reacting with it, allowing the walkers to deeply penetrate pores before reacting, corresponding to chemistry-limited conditions and a slow reaction rate K . For r near unity, an encounter almost always leads to reaction and only the most exposed parts of the cluster are consumed, corresponding to diffusion-limited oxidation and a high reaction rate K_d . In this way, the reaction probability is just the overall reaction rate normalized to unity; $r = K/K_d = K_c/(K_c + K_d)$.

5. Model tuning

The model is tuned by comparing with data from combustion of a finely graded (38-45 micron diameter with median diameter 39 microns) lightly swelling Montana lignite studied experimentally by Sarofim (9). Their microscopic examination of these particles indicates that the mineral matter is distributed as separate inclusions comprising about 8% of the coal with a maximum weight fraction at a diameter of 2 microns. Lacking detailed information about the small amount of swelling during devolatilization, we simply use the initial coal particle diameter as the diameter relevant to char oxidation. Particle surface temperatures T_s typically exceed bulk gas temperatures T_b by about 200 K (2).

To facilitate careful comparison with the experiments, the mineral masses assigned to bonds in the cluster are chosen to obey the distribution of the mineral inclusions measured in the experiments, which is apparently independent of coal particle size over the relevant range of particle sizes. In particular, the number of required inclusions in each of six bins of width 0.5 microns is determined from Figure 6 of Sarofim (9) based on the overall diameter d of the assumed spherical coal particle, the mineral fraction (8%), and the approximately equal density 3.5 g cm^{-3} of char and mineral matter. The mass of the assumed spherical inclusions in each bin follows from the mean bin diameter. The N mineral inclusions required by the procedure are then randomly assigned to N bonds in the cluster ($N = 1749$ for $d = 39$ microns), and the remaining bonds in the cluster are assigned zero mineral mass. Our clusters typically contain from N to $1.1 N$ bonds. The largest simulated particle diameter was 44 microns.

We use the conditions $d = 39$ microns and $T_s = 2000$ K to tune the cluster compactness and the method of mineral matter reallocation during combustion. For unit compactness ($R = 1$) and for weak mineral cohesion (limit II), we obtain a distribution with a narrow peak in the ash mass fraction per micron at about 2.5 microns compared with a corresponding median diameter of 9 microns for comparable conditions in the experiments [Figure 14 of Ref. (9), $T_b = 1830$ K]. For higher compactness ($R = 2$) and for strong mineral cohesion (limit I), the median diameter rises to about 4.4 microns (Figure 1) and the width of the distribution is comparable to that of the experiments. For $R = 3$ and strong mineral cohesion, we obtain a very broad distribution centered very roughly at 8 microns. To better facilitate the study of the shifts in median diameter with temperature and particle diameter, we henceforth employ the more sharply peaked intermediate compactness $R = 2$ in the strong mineral cohesion limit. Our choice of compactness may correspond more closely to more porous chars, such as bituminous chars, than to the lignite of the experiments. We believe however that the directions and relative magnitudes of the shifts in the median diameter due to changing temperature and particle diameter should be applicable to a wide range of porosities including the lignite of the experiments, since these shifts arise from different oxidation regimes applied to the same types of particles. Our choice of strong mineral cohesion seems consistent with current understanding of the process of mineral coalescence.

6. Predictions and comparisons with experiments

To illustrate the dependence of the ash particle size distribution on temperature, Figure 1 shows our simulated mass-weighted ash size distributions for $d = 39$ microns at $T_s = 1500, 2000,$ and 2500 K. The data points are the output of the simulations; the solid traces are fifth-order polynomial fits to the data. The cluster used in all three simulations had 1781 bonds including 1749 mineral inclusions. The data show a systematic shift toward larger ash particles with increasing temperature (Figure 1); median diameters deduced from the fits are 3.7, 4.4, and 4.8 microns. A significant decrease in the overall number of ash particles from 171 at $T_s = 1500$ K to 115 at $T_s = 2500$ K (Table 1) accompanies the shift toward larger ash particles. Physically, the larger ash particles result from a decrease in pore wall oxidation and a corresponding decrease in fragmentation as the oxidation approaches the diffusion-limited regime with increasing temperature. The experimental data of Sarofim et al. (9) do not show an clear shift toward larger ash particles for increasing temperatures. Even so, for the case of $d = 39$ microns, the experimental ratio 0.86 between median ash particle diameters at bulk gas temperatures $T_b = 1830$ K and $T_b = 1250$ K [deduced from Figure 14 of Ref. (9)] compares well with our ratio 0.84 deduced from the median diameters at the corresponding surface temperatures $T_s = 2000$ K and $T_s =$

1500 K. The experimental overall number of ash particles 160 at $T_s = 2000$ K [estimated from data for $d = 53-63$ and $75-90$ microns and bulk temperatures $T_b = 1750$ K, Ref. (10)] is comparable to our value of 121 (Table 1).

To determine the dependence of the ash particle size distribution on initial particle diameter, Figure 2 shows our simulated ash size distributions for $d = 34, 39,$ and 44 microns at $T_s = 2000$ K. The corresponding clusters have 1162 (1152), 1781 (1749), and 2665 (2509) bonds, where parentheses enclose the numbers of bonds assigned mineral inclusions. Over this range of diameters, no clear trend in the ash particle size distribution is discernible (Figure 2). The increase with diameter of the overall number of ash fragments (Table 1) reflects the larger number of mineral inclusions in particles of larger diameter. The initial values of the reaction probability for these particles are 0.58, 0.61, and 0.64, respectively.

7. Conclusions

This paper presents, to our knowledge, the first model predicting ash distributions resulting from char oxidation and fragmentation incorporating the three regimes of oxidation. The model yields overall numbers of ash particles and shifts in ash particle distributions which agree with experiments on a Montana lignite. Since the sparse cluster morphologies studied in this paper underestimate the experimental median ash particle size, these morphologies may correspond best to more porous bituminous chars. Over the range of particle diameters studied (34-44 microns), the model predicts no variation in the median ash diameter with initial particle size. Further simulations of denser cluster morphologies and over larger diameter ranges are underway.

Experiments on the process of molten mineral matter reallocation during combustion would be very useful in connection with our ongoing simulations. Additionally, since significant swelling and morphological changes may occur during devolatilization, experiments on combustion of well-characterized chars (including sizes, porosities, and mineral matter distributions) would be useful.

The model provides a flexible and powerful framework in which to study the separate and combined effects of initial mineral content and distribution, coal type and morphology, oxygen concentration, temperature, and particle size on the final ash size distribution. It can be used to compare and correlate experimental data, as well as to study parameter sensitivities that are difficult to explore experimentally.

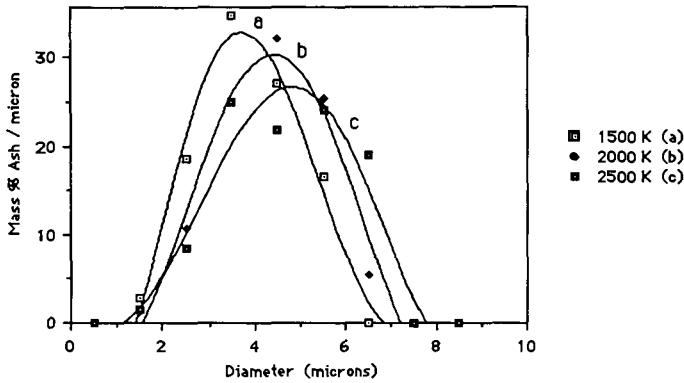


Figure 1. Mass-weighted ash size distribution for simulated coal particle diameter 39 microns and surface temperatures 1500, 2000, and 2500 K.

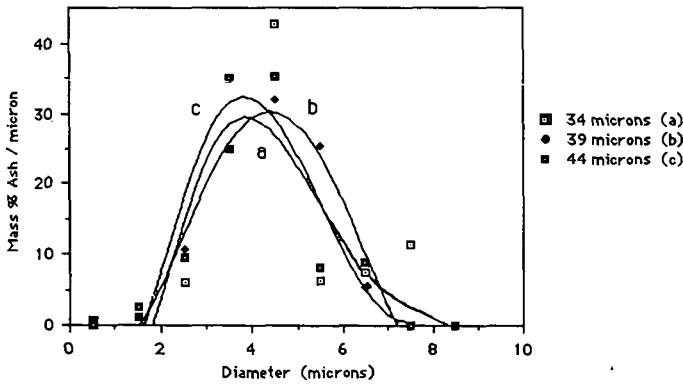


Figure 2. Mass-weighted ash size distribution for simulated coal particle diameters 34, 39, and 44 microns at surface temperature 2000 K.

d (μm)	T_s (K)	Ash particle size range (microns)									total
		0-1	1-2	2-3	3-4	4-5	5-6	6-7	7-8	8-9	
39	1500	25	34	53	39	15	5				171
39	2000	24	17	30	26	16	17	1			121
39	2500	27	18	23	26	11	7	3			115
34	2000	12	12	11	17	16	1	1	1		71
44	2000	45	48	36	54	14		2			216

Table 1. Numbers of ash particles of different sizes ranges for simulated coal particles of diameter d and surface temperature T_s .

8. References

- (1) Sundback, C. A., Beer, J. M., and Sarofim, A. F., 1985, Fragmentation Behavior of Single Coal Particles in a Fluidized Bed, *Twentieth Symposium (International) on Combustion*. The Combustion Institute, Pittsburgh, 1495-1504.
- (2) Mitchell, R. E. and McLean, W. J., 1982, On the Temperature and Reaction Rate of Burning Pulverized Fuels. *Nineteenth Symposium (International) on Combustion*. The Combustion Institute, Pittsburgh, 1113-1122.
- (3) Field, M. A., Gill, D. W., Morgan, B. B., and Hawksley, P. G. W., 1967, *Combustion of Pulverized Coal*, BCURA, Chap. 6 186-195.
- (4) Reyes, S. and Jensen, K. F., 1986a, Percolation Concepts in Modelling of Gas-solid Reactions I. Application to Char Gasification in the Kinetic Regime. *Chem. Eng. Sci.* **41**, 333-343.
- (5) Reyes, S. and Jensen, K. F., 1986b, Percolation Concepts in Modelling of Gas-solid Reactions I. Application to Char Gasification in the Diffusion Regime. *Chem. Eng. Sci.* **41**, 345-354.
- (6) Kerstein, A. R. and Bug, A. L. R., 1986, Scaling Theory of Pore Growth in a Reactive Solid, *Phys. Rev. B* **34**, 1754-1761.
- (7) Sahimi, M., and Tsotsis, T. T., 1988, Statistical Modeling of Gas-solid Reaction with Pore Volume Growth: Kinetic Regime. *Chem. Eng. Sci.*, **43**, 113-121.
- (8) Kerstein, A. R. and Edwards, B. F., 1986, Percolation Model for Simulation of Char Oxidation and Fragmentation Time-Histories, *Chem. Eng. Sci.*, **42**, 1629-1634.
- (9) Sarofim, A. F., Howard, J. B., and Padia, A. S., 1977, The Physical Transformation of the Mineral Matter in Pulverized Coal Under Simulated Combustion Conditions, *Combustion Science & Technology*, **16**, 187-204.
- (10) Helble, J. J. and Sarofim, A. F., 1987, Influence of Char Fragmentation on Ash Particle Size Distribution, preprint.
- (11) Holve, D. J., 1986, In Situ Measurement of Flyash Formation from Pulverized Coal, *Combustion Science & Technology*, **44**, 269-287.
- (12) Sahimi, M., and Tsotsis, T. T., 1987, Dynamic Scaling for the Fragmentation of Reactive Porous Media, *Phys. Rev. Lett.*, **59**, 888-891.
- (13) Smith, I. W., 1971, The Kinetics of Combustion of Size Graded Pulverized Fuels in the Temperature Range 1200-2700 K, *Combustion & Flame*, **17**, 304-313.
- (14) Walker, P. L., Ruskino, F., Austin, L. G., 1967, Gas Reactions of Carbon, *Advances in Catalysis*, **11**, 133-221.
- (15) Field, M. A., 1970, Measurements of the Effect of Rank on Combustion Rates of Pulverised Coal, *Combustion & Flame*, **14**, 237-248.
- (16) Wall, T. F., Gururajan, V. S., 1986, Combustion Kinetics and the Heterogeneous Ignition of Pulverized Coal, *Combustion & Flame*, **66**, 151-157.